

Structural dependence of effective area and mode field diameter for holey fibers

M. Koshiba and K. Saitoh

Hokkaido University, North 13 West 8, Kita-ku, Sapporo, 060-8628, Japan
koshiba@ice.eng.hokudai.ac.jp

Abstract: A rigorous full-vector finite element method is effectively applied to evaluating the effective area A_{eff} and the mode field diameter (MFD) of holey fibers (HFs) with finite cross sections. The effective modal spot size (a half of MFD), w_{eff} , is defined with the help of the second moment of the optical intensity distribution. The influence of hole diameter, hole pitch, operating wavelength, and number of rings of air holes on A_{eff} and w_{eff} is investigated in detail. As a result, it is shown that A_{eff} and w_{eff} are almost independent of the number of hole rings and that the relation $A_{eff} = \pi w_{eff}^2$, which is frequently utilized in the conventional optical fibers, does not always hold, especially in smaller air-filling fraction and/or longer wavelength regions. In addition, we find that for HFs with large air holes operating at longer wavelengths, the mode profiles of the two linearly polarized fundamental modes are significantly different from each other, even though they are degenerate. Using the values of A_{eff} and w_{eff} obtained here, the beam divergence and the nonlinear phase shift are calculated and are compared with the earlier experimental results.

©2003 Optical Society of America

OCIS codes: (060.2270) Fiber Characterization; (060.2280) Fiber design and fabrication; (060.2430) Fibers, single mode

References and links

1. J. Broeng, D. Mogilevstev, S.E. Barkou, and A. Bjarklev, "Photonic crystal fibers: A new class of optical waveguides," *Opt. Fiber Technol.* **5**, 305-330, (1999).
2. T.A. Birks, J.C. Knight, B.J. Mangan, and P.St.J. Russell, "Photonic crystal fibers: An endless variety," *IEICE Trans. Electron.* **E84-C**, 585-592, (2001).
3. T.M. Monro, D.J. Richardson, N.G.R. Broderick, and P.J. Bennett, "Modeling large air fraction holey optical fibers," *J. Lightwave Technol.* **18**, 50-56, (2000).
4. N.A. Mortensen, "Effective area of photonic crystal fibers," *Opt. Express* **10**, 341-348, (2002), <http://www.opticsexpress.org/abstract.cfm?URI=OPEX-10-7-341>
5. T.M. Monro, V. Finazzi, W. Belardi, K.M. Kiang, J.H. Lee, and D.J. Richardson, "Highly nonlinear holey optical fibers: design, manufacture and device applications," *Proc. European Conf. Opt. Commun., Symposium 1.5.* (2002).
6. M. Koshiba and Y. Tsuji, "Curvilinear hybrid edge/nodal elements with triangular shape for guided-wave problems," *J. Lightwave Technol.* **18**, 737-743, (2000).
7. K. Saitoh and M. Koshiba, "Full-vectorial finite element beam propagation method with perfectly matched layers for anisotropic optical waveguides," *J. Lightwave Technol.* **19**, 405-413, (2001).
8. K. Saitoh and M. Koshiba, "Full-vectorial imaginary-distance beam propagation method based on finite element scheme: Application to photonic crystal fibers," *IEEE J. Quantum Electron.* **38**, 927-933, (2002).
9. T.P. White, R.C. McPhedran, C.M. de Sterke, L.C. Botten, and M.J. Steel, "Confinement losses in microstructured optical fibers," *Opt. Lett.* **26**, 1660-1662, (2001).
10. V. Finazzi, T.M. Monro, and D.J. Richardson, "Confinement loss in highly nonlinear holey optical fibers," *Proc. Optical Fiber Commun. Conf. ThS4.* (2002).
11. M.J. Gander, R. McBride, J.D.C. Jones, T.A. Birks, J.C. Knight, P.St.J. Russell, P.M. Blanchard, J.G. Burnett, and A.H. Greenaway, "Measurement of the wavelength dependence of beam divergence for photonic crystal fiber," *Opt. Lett.* **24**, 1017-1019, (1999).

12. N.A. Mortensen, J.R. Folken, P.M.W. Skovgaard, and J. Broeng, "Numerical aperture of single-mode photonic crystal fibers," *IEEE Photon. Technol. Lett.* **14**, 1094-1096, (2002).
13. J.H. Lee, P.C. Teh, Z. Yusoff, M. Ibsen, W. Belardi, T.M. Monro, and D.J. Richardson, "A holey fiber-based nonlinear thresholding devices for optical CDMA receiver performance enhancement," *IEEE Photon. Technol. Lett.* **14**, 876-878, (2002).
14. J.W.H. Liu, "The multifrontal method for sparse matrix solutions: theory and practice," *SIAM Rev.* **34**, 82-109, (1992).
15. G. Agrawal, *Nonlinear Fiber Optics*, Academic Press (San Diego, CA), 2nd Edition (1995).
16. K. Petermann, "Constraints for fundamental-mode spot size for broadband dispersion-compensated single-mode fibers," *Electron. Lett.* **19**, 712-714, (1983).
17. M.J. Steel, T.P. White, C. Martijn de Sterke, R.C. McPhedran, and L.C. Botten, "Symmetry and degeneracy in microstructured optical fibers," *Opt. Lett.* **26**, 488-490, (2001).
18. M. Koshihara and K. Saitoh, "Numerical verification of degeneracy in hexagonal photonic crystal fibers," *IEEE Photon. Technol. Lett.* **13**, 1313-1315, (2001).
19. K. Hayata, M. Koshihara, and M. Suzuki, "Modal spot size of axially nonsymmetrical fibers," *Electron. Lett.* **22**, 127-129, (1986).
20. M. Koshihara and K. Saitoh, "Polarization-dependent losses in actual holey fibers," *IEEE Photon. Technol. Lett.* **15**, 691-693, (2003).

1. Introduction

Photonic crystal fibers, also called holey fibers (HFs), have been one of the most interesting developments in recent fiber optics [1],[2].

The effective area A_{eff} is a quantity of great importance in fiber optics. It was originally introduced as a measure of nonlinearities; a small effective area would be useful for enhancing nonlinear effects. Often a large effective area is desired, and then high powers can be transmitted without introducing any unwanted nonlinear effects in the fiber. Although several authors have reported theoretical studies of effective area for HFs [3],[4], the influence of the extent of the confining air hole region on effective area has not been investigated. More recently, Monro *et al.* have reported a pioneering work regarding the effective area of HFs with a few rings of air holes and have claimed that A_{eff} is effectively independent of the number of hole rings [5]. However, in [5] the number of rings of air holes has been limited to 2 to 4 and the operating wavelength has been fixed to 1550 nm.

The mode field diameter (MFD) is another important parameter in the context of beam divergence, splice loss, bending loss, source-to-fiber coupling efficiency, and so on. Although the MFD can be related to the effective area through the relation $A_{eff} = \pi w_{eff}^2$ with w_{eff} being the effective modal spot size (a half of MFD), which is frequently utilized in the conventional optical fibers, this relation is valid only for close-to-Gaussian modes in ordinary axially symmetrical fibers and its applicability to HFs has not been fully investigated so far.

In this paper, using a rigorous full-vector finite element method [6]-[8], A_{eff} and MFD of HFs with finite cross sections are evaluated. In order to treat axially nonsymmetrical fibers such as HFs with air holes arranged in a triangular lattice in the cladding region, the second moment of the optical intensity distribution is introduced as the definition of w_{eff} . The influence of hole diameter, hole pitch, operating wavelength, and number of hole rings on A_{eff} and w_{eff} is investigated in detail, including confinement losses arising from the leaky nature of HFs with finite cross sections. As a result, it is shown that in contrast with the confinement losses which is strongly dependent of the number of hole rings [8]-[10], A_{eff} and w_{eff} are almost independent of it and that the relation $A_{eff} = \pi w_{eff}^2$ does not always hold, especially in smaller air-filling fraction and/or longer wavelength regions. In addition, we find that for HFs with large air holes operating at longer wavelengths, the mode profiles of the horizontally polarized and vertically polarized fundamental modes are significantly different from each other, even though these two linearly polarized modes are degenerate in strict sense. Using the values of A_{eff} and w_{eff} obtained here, the beam divergence and the nonlinear phase shift are calculated and are compared with the earlier experimental results [11]-[13].

2. Analysis method

We consider a HF with finite cross section as shown in Fig. 1, where x and y are the transverse directions, z is the propagation direction, d is the hole diameter, and Λ is the hole pitch. Anisotropic perfectly matched layers (PMLs) [7],[8] are incorporated as absorbing boundary conditions to evaluate confinement losses. From Maxwell's equations the following vector wave equation is derived [8]:

$$\nabla \times ([s]^{-1} \nabla \times \mathbf{E}) - k_0^2 n^2 [s] \mathbf{E} = \mathbf{0} \quad (1)$$

where \mathbf{E} is the electric field vector, n is the refractive index, $[s]$ is the PML matrix, and $[s]^{-1}$ is an inverse matrix of $[s]$.

When applying a full-vector FEM to HFs, a curvilinear hybrid edge/nodal element [6] as shown in Fig. 2 is very useful for avoiding spurious solutions and for accurately modeling curved boundaries of circular air holes. For the axial field, E_z , a nodal element with six variables, E_{z1} to E_{z6} , is employed, while for the transverse fields, E_x and E_y , an edge element with eight variables, E_{t1} to E_{t8} , is employed, resulting in significantly fast convergence of solutions [6].

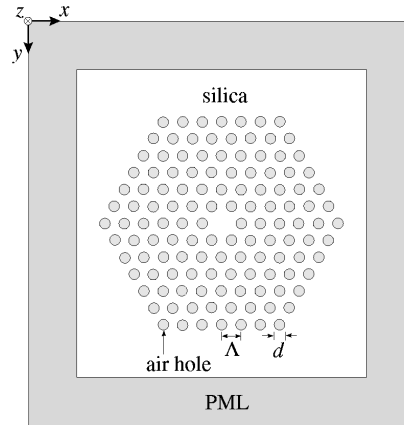


Fig. 1. Holey fiber with finite cross section.

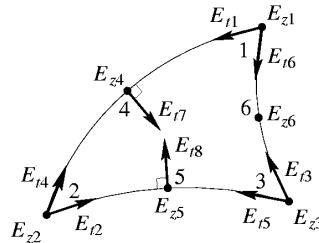


Fig. 2. Curvilinear hybrid edge/nodal element.

Dividing the fiber cross section into curvilinear hybrid edge/nodal elements, we expand the transverse and axial fields in each element as

$$\mathbf{E} = \begin{bmatrix} E_x \\ E_y \\ E_z \end{bmatrix} = \begin{bmatrix} \{U(x, y)\}^T \{E_t\}_e \exp(-j\beta z) \\ \{V(x, y)\}^T \{E_t\}_e \exp(-j\beta z) \\ j\beta \{N(x, y)\}^T \{E_z\}_e \exp(-j\beta z) \end{bmatrix} \quad (2)$$

where β is the propagation constant, $\{E_t\}_e$ and $\{E_z\}_e$ are, respectively, the edge and the nodal variables for each element e , $\{U\}$ and $\{V\}$ are the shape function vectors for edge elements, $\{N\}$ is the shape function vector for nodal elements, and T denotes a transpose.

Applying the standard finite element technique to Eq. (1), we can obtain the following eigenvalue equation:

$$[K]\{E\} = \beta^2[M]\{E\} \quad (3)$$

with

$$\{E\} = \begin{bmatrix} \{E_t\} \\ \{E_z\} \end{bmatrix} \quad (4)$$

where $\{E\}$ is the global electric field vector and the finite element matrices $[K]$ and $[M]$ are given in [8]. Utilizing sparse nature of $[K]$ and $[M]$, Eq. (3) is solved with the multifrontal method [14].

The area of the fundamental mode is clearly related to the effective area of the fiber core, A_{eff} , for which we use the following definition [15]:

$$A_{eff} = \frac{\left(\iint_S |E_t|^2 dx dy \right)^2}{\iint_S |E_t|^4 dx dy} \quad (5)$$

where E_t is the transverse electric field vector and S denotes the whole fiber cross section. Using the eigenvector $\{E\}$ corresponding to the eigenvalue β^2 obtained from Eq. (3) and noting the relation of Eq. (2), A_{eff} is calculated as

$$A_{eff} = \frac{\left[\sum_e \iint_e I_e(x, y) dx dy \right]^2}{\sum_e \iint_e I_e^2(x, y) dx dy} \quad (6)$$

where \sum_e extends over all different elements and the optical intensity distribution for each element, I_e , is given by

$$I_e(x, y) = \left| \{U(x, y)\}^T \{E_t\}_e \right|^2 + \left| \{V(x, y)\}^T \{E_t\}_e \right|^2. \quad (7)$$

In HFs the two linearly polarized fundamental modes exist. One is polarized in the horizontal (x) direction and the other in the vertical (y) direction, and these two fundamental modes are degenerate [17],[18]. As is well-known, the mode profile of the fundamental mode in step-index fibers can be well approximated with a Gaussian shape, and the MFD is usually calculated using the Petermann's definition [16]. However, the Petermann's definition cannot be applied to the MFD of HFs because the mode profile in such fibers is considerably deformed by the existence of air holes arranged in a triangular lattice and may be different from that in ordinary axially symmetrical fibers. So, we adapt the second moment of the optical intensity distribution as the definition of modal spot size (a half of MFD) for HFs which is very useful for axially nonsymmetrical fibers. According to [19], the modal spot sizes in the x and y directions, w_x and w_y , are given by

$$w_x^2 = 4 \frac{\iint_S (x - x_c)^2 |E_t|^2 dx dy}{\iint_S |E_t|^2 dx dy} = 4 \frac{\sum_e \iint_e (x - x_c)^2 I_e(x, y) dx dy}{\sum_e \iint_e I_e(x, y) dx dy} \quad (8)$$

$$w_y^2 = 4 \frac{\iint_S (y - y_c)^2 |\mathbf{E}_t|^2 dx dy}{\iint_S |\mathbf{E}_t|^2 dx dy} = 4 \frac{\sum_e \iint_e (y - y_c)^2 I_e(x, y) dx dy}{\sum_e \iint_e I_e(x, y) dx dy} \quad (9)$$

where x_c and y_c are, respectively, the x and y coordinates of the center of the field distribution, which are calculated as

$$x_c = \frac{\iint_S x |\mathbf{E}_t|^2 dx dy}{\iint_S |\mathbf{E}_t|^2 dx dy} = \frac{\sum_e \iint_e x I_e(x, y) dx dy}{\sum_e \iint_e I_e(x, y) dx dy} \quad (10)$$

$$y_c = \frac{\iint_S y |\mathbf{E}_t|^2 dx dy}{\iint_S |\mathbf{E}_t|^2 dx dy} = \frac{\sum_e \iint_e y I_e(x, y) dx dy}{\sum_e \iint_e I_e(x, y) dx dy}. \quad (11)$$

In the curvilinear elements with triangular shape the Cartesian coordinates, x and y , are, in general, approximated with quadratic polynomials using the local coordinates, L_1 , L_2 , and L_3 , which are also called the area coordinates for the rectilinear elements with triangular shape [6]. Noting that all the shape function vectors, $\{U\}$, $\{V\}$, and $\{N\}$, are also given as the functions of L_1 , L_2 , and L_3 , Eqs. (6) and (8) to Eq. (11) can be easily and accurately evaluated by using the well-established numerical integration formulas (see Eq. (16) in [6]).

As will be demonstrated in Section 4, the modal spot sizes in the x and y directions, w_x and w_y , are, in general, different from each other, and so we define the following effective modal spot size w_{eff} :

$$w_{eff}^2 = \frac{w_x^2 + w_y^2}{2}. \quad (12)$$

With this definition, w_{eff} remains the $1/e^2$ intensity radius (namely, the $1/e$ field radius) for a Gaussian profile. A similar definition has been introduced to the measurement of the far-field intensity profile with a Gaussian beam approximation [11].

3. Effective area and confinement loss

HFs are usually made from pure silica, and so the guided modes are inherently leaky because the core index is the same as the index of the outer cladding region without air holes. Figure 3 shows the normalized effective area and the normalized confinement loss of the fundamental mode in HFs with finite cross sections, taking the ratio of hole diameter to pitch, d/Λ , as a parameter, where N is the number of rings of air holes, the background silica index n is assumed to be 1.45, and the normalized confinement loss in dB, $L_c\Lambda$, is defined as

$$L_c\Lambda = 8.686 \text{ Im}[\beta\Lambda]. \quad (13)$$

Here Im stands for the imaginary part. For example, assuming the value of $L_c\Lambda$ to be 10^{-8} dB, the confinement loss L_c becomes 10 dB/km for $\Lambda = 1 \mu\text{m}$ and 1 dB/km for $\Lambda = 10 \mu\text{m}$.

As expected, increasing the air-hole size, the mode becomes more confined, and thus, the effective area and the confinement loss are both reduced. Also, increasing the number of rings of air holes, the confinement loss is significantly reduced. On the other hand, the effective area is almost independent of the number of hole rings, as claimed by Monro *et al.* [5]. This seems to be due to the fact that even if $A_{eff}/\Lambda^2 \cong \pi$, the spread of effective area is in the order of Λ corresponding to the position of the first ring. In Fig. 3(f), the results of a rigorous full-vector multipole method (MM) [5] are also plotted. Our results agree well with those of MM, showing the reliability of a full-vector FEM with PMLs.

Figure 3 is a general “map” of the effective area which can be used for designing various HFs, such as ultra-low nonlinearity HFs and high nonlinearity HFs with desired confinement loss properties. If, for example, the operating wavelength is given, the effective area and the confinement loss can to a large extent be tailored via the choice of hole pitch, hole size, and number of hole rings.

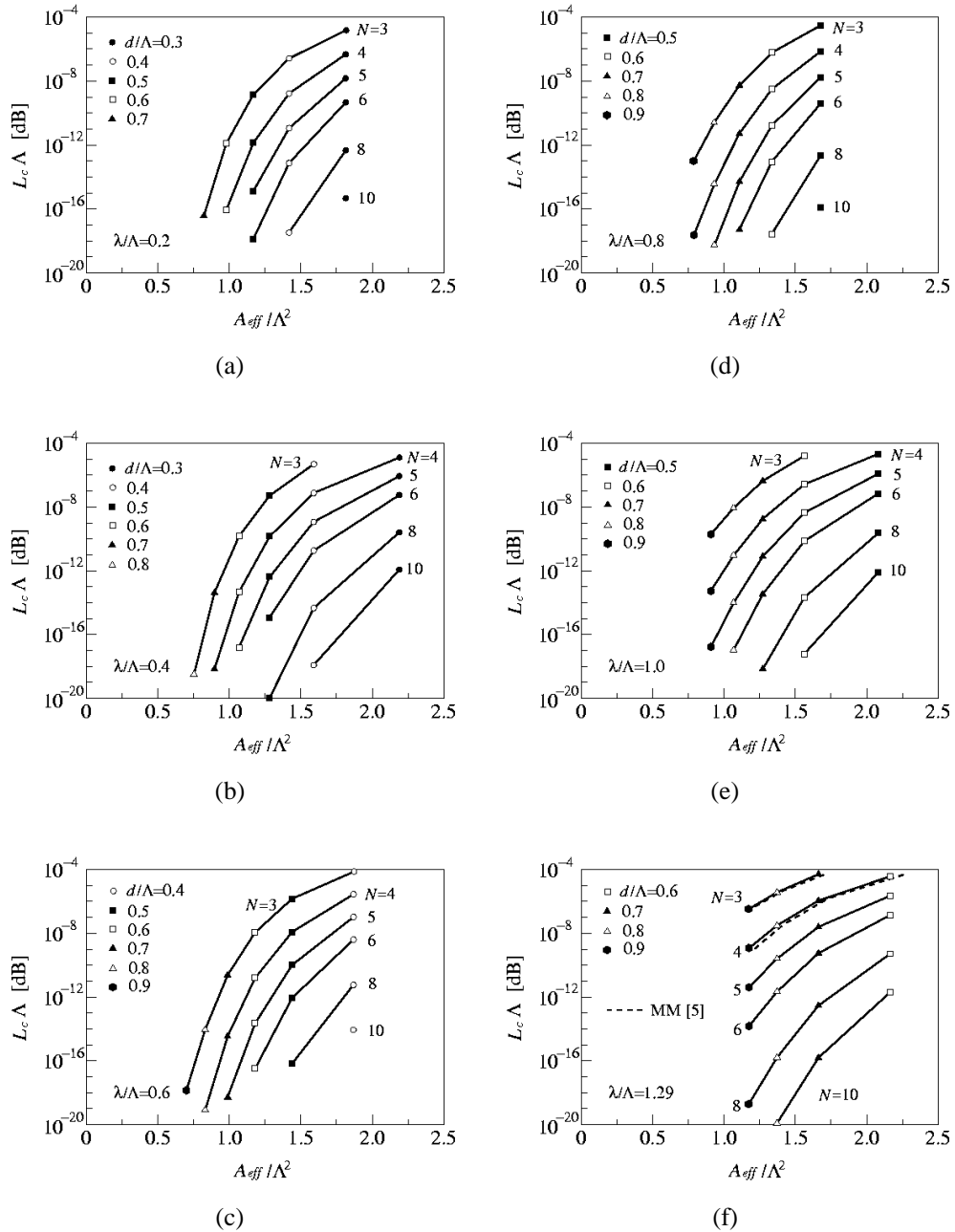


Fig. 3. Effective area and confinement loss of holey fibers operating at the wavelength of (a) $\lambda/\Lambda = 0.2$, (b) $\lambda/\Lambda = 0.4$, (c) $\lambda/\Lambda = 0.6$, (d) $\lambda/\Lambda = 0.8$, (e) $\lambda/\Lambda = 1.0$, and (f) $\lambda/\Lambda = 1.29$.

4. Effective area and mode field diameter

As described in the previous section, the effective area is almost independent of the number of hole rings, and here, we consider a HF with ten rings.

Figure 4 shows the relationship between effective area A_{eff} and mode field diameter (MFD) as a function of wavelength for different hole sizes, where the MFD is expressed in the form of πw_{eff}^2 with w_{eff} (a half of MFD) being the effective modal spot size given in Eq. (12). Roughly speaking, the results for A_{eff} and πw_{eff}^2 are similar, but in a strict sense, the relation $A_{eff} = \pi w_{eff}^2$, which is frequently adopted to the conventional optical fibers, does not hold, especially in smaller air-filling fraction and/or larger wavelength regions. This suggests that the mode field in these cases cannot be approximated by a simple circularly symmetric Gaussian shape. In fact, Fig. 5 shows the intensity profiles of the fundamental modes in a HF with air-hole size of $d/\Lambda = 0.3$ at $\lambda/\Lambda = 0.2$, where the intensity contours are spaced by 1 dB. The left and right profiles show the principal field components of the horizontally polarized and vertically polarized modes, respectively, which are degenerate [17],[18]. These intensity profiles are very similar. As is well-known, these linearly polarized modes have six-fold rotational symmetry. We can see the deviation from the typical circular shape, resulting in a failure to rely on the relation $A_{eff} = \pi w_{eff}^2$ to express MFD from A_{eff} .

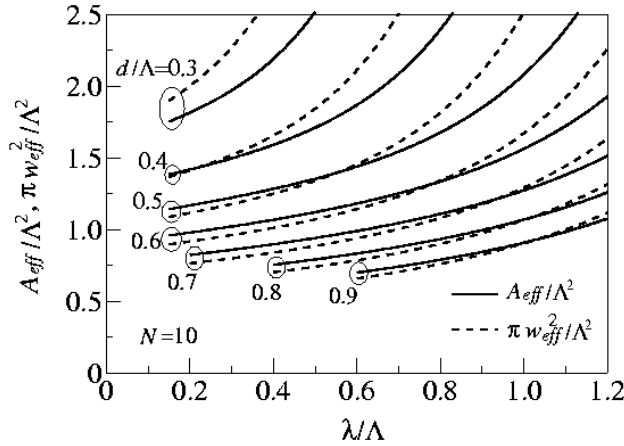


Fig. 4. Relationship between effective area and mode field diameter as a function of wavelength.

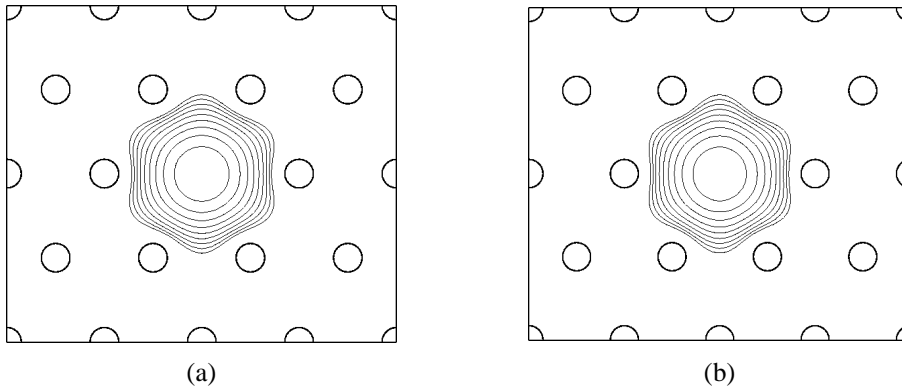


Fig. 5. Intensity profile of (a) horizontally polarized and (b) vertically polarized modes in a holey fiber with $d/\Lambda = 0.3$ at $\lambda/\Lambda = 0.2$, where $|E_x|^2$ in (a) and $|E_y|^2$ in (b) are expressed in the intensity contours spaced by 1 dB.

Figure 6 shows the relationship among three kinds of modal spot sizes for the horizontally polarized mode, w_{eff} , w_x , and w_y , as a function of wavelength. For the vertically polarized mode, the values of w_x and w_y are interchanged. The results of the effective modal spot size w_{eff} are the same as those in Fig. 4. The modal spot sizes in the x and y directions, w_x and w_y , are, respectively, obtained from Eqs. (8) and (9). It is worth noting that for HF with large air holes operating at longer wavelengths, these values are significantly different from each other. This suggests that the mode field in these cases may be considerably deviated from that in ordinary axially symmetrical fibers. Figure 7 shows the intensity profiles of the horizontally polarized and vertically polarized modes in a HF with $d/\Lambda = 0.9$ at $\lambda/\Lambda = 1.2$, where the intensity contours are spaced by 1 dB. Surprisingly, in contrast to those in Fig. 5, these intensity profiles are entirely different from each other, even though these two linearly polarized modes are degenerate. They have no longer six-fold rotational symmetry. Such curious mode shapes have not been reported so far, to our knowledge. Traditional methods, which rely on Gaussian optics to estimate the splice loss, source-to-fiber coupling efficiency, and so on, would fail in these cases, and therefore, more rigorous numerical methods may be required.

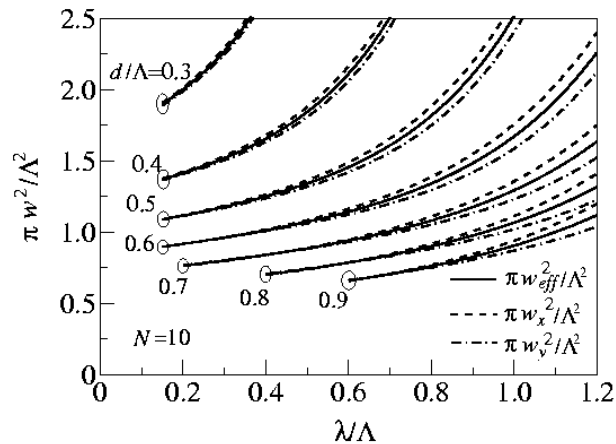


Fig. 6. Relationship among three kinds of modal spot sizes as a function of wavelength.

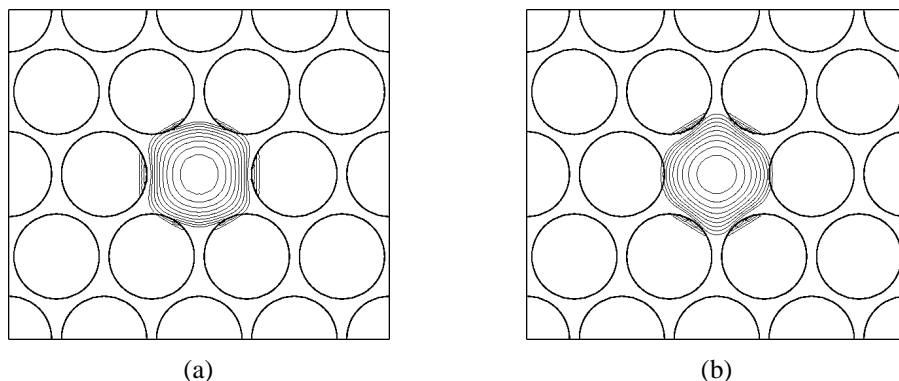


Fig. 7. Intensity profile of (a) horizontally polarized and (b) vertically polarized modes in a holey fiber with $d/\Lambda = 0.9$ at $\lambda/\Lambda = 1.2$, where $|E_x|^2$ in (a) and $|E_y|^2$ in (b) are expressed in the intensity contours spaced by 1 dB.

5. Beam divergence and nonlinear phase shift

In this section, using the values of effective area and MFD obtained here, the beam divergence and the nonlinear phase shift of HFs are calculated and are compared with the earlier experimental results [11]-[13].

Figure 8 shows the beam divergences of HFs with hole pitch $\Lambda = 2.39 \mu\text{m}$ and hole diameter $d/\Lambda = 0.26$ and with $\Lambda = 7.2 \mu\text{m}$ and $d/\Lambda = 0.53$, where the beam divergence θ is given by

$$\theta = \tan^{-1} \frac{\lambda}{\pi w_{eff}} \quad (14)$$

with w_{eff} being the effective modal spot size in (12) and λ being the operating wavelength. In Fig. 8, assuming the relation $A_{eff} = \pi w_{eff}^2$, the beam divergences obtained from A_{eff} , $\theta = \tan^{-1}(\lambda/\sqrt{\pi A_{eff}})$, are also plotted. For a relatively large air-hole case, $d/\Lambda = 0.53$ and $\lambda/\Lambda < 0.14$, the relation $A_{eff} = \pi w_{eff}^2$ is approximately satisfied (see Fig. 4), and so the beam divergence obtained from A_{eff} is very similar to that obtained from w_{eff} . For a considerably small air-hole case, $d/\Lambda = 0.26$ and $\lambda/\Lambda < 0.42$, on the other hand, the relation $A_{eff} = \pi w_{eff}^2$ does not hold (see again Fig. 4). Irrespective of air hole sizes, the beam divergences obtained from w_{eff} , in other word, MFD, are in good quantitative agreement with the experimental ones [11],[12]. From Fig. 8, we can say that the beam divergence is not well quantified in terms of the concept of effective area.

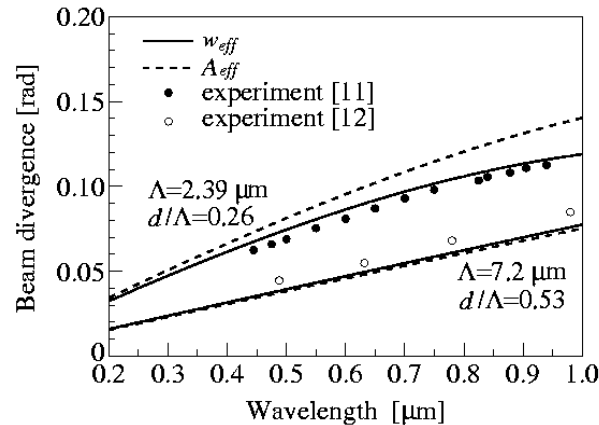


Fig. 8. Beam divergences of holey fibers.

Then, we consider a highly nonlinear HF as shown in Fig. 9 [13]. In order to estimate A_{eff} and MFD of such an actual fiber, the real-model simulation [20] is indispensable. In the ideal structure, the two linearly polarized fundamental modes are degenerate [17],[18], and so A_{eff} and MFD are independent of the polarization states. In the actual fiber structure, on the other hand, they depend on the polarization states. Figure 10 shows the values of A_{eff} and πw_{eff}^2 of the two fundamental modes called slow-axis and fast-axis modes as a function of wavelength. The real part of propagation constant of the slow-axis mode is slightly larger than that of the fast-axis mode. In Fig. 10 the modal birefringence is also plotted. This fiber exhibits very small effective area and large birefringence of the order of 10^{-3} . The calculated A_{eff} and the modal birefringence are in good agreement with the experimental ones [13]. In this fiber the

relation $A_{eff} = \pi w_{eff}^2$ is approximately satisfied because the ratio of hole diameter to pitch is relatively large. Figure 11 shows the normalized phase shift given by

$$\phi_{SPM} = \frac{4\pi n_2 P}{\lambda A_{eff}} \quad (15)$$

where n_2 is the nonlinear-index coefficient for pure silica, P is the signal power, and the operating wavelength is taken as 1.553 μm . The calculated ϕ_{SPM} for the slow-axis mode agree well with the experimental one [13].

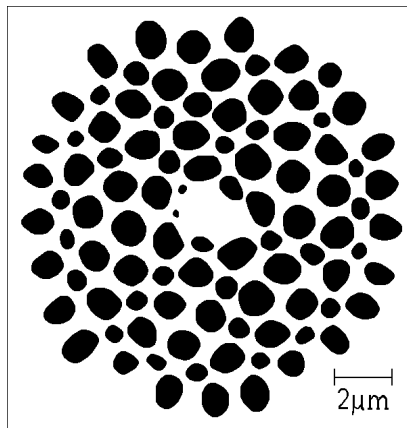


Fig. 9. Highly nonlinear holey fiber [13].

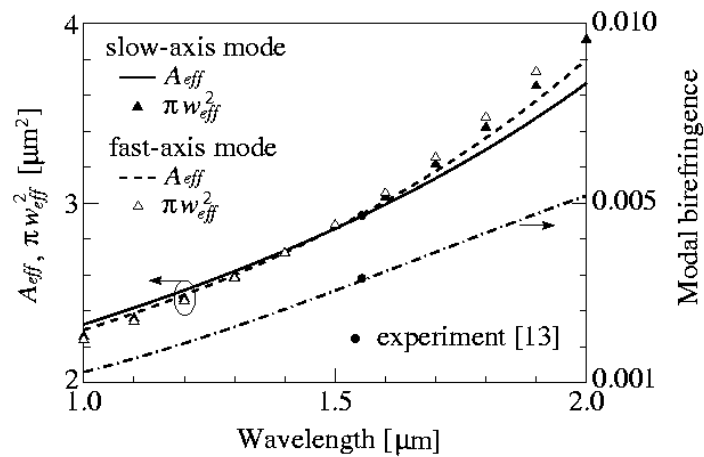


Fig. 10. Effective area, modal spot size, and birefringence of a holey fiber shown in Fig. 9.

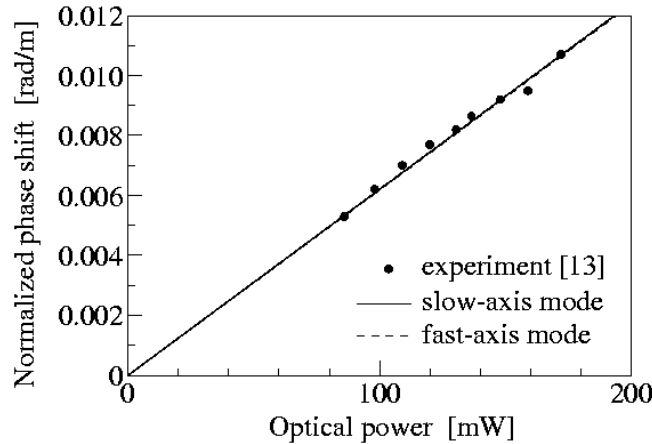


Fig. 11. Nonlinear phase shift of a holey fiber shown in Fig. 9.

6. Conclusion

Using a rigorous full-vector finite element method, the effective area A_{eff} and the mode field diameter (MFD) of holey fibers (HFs) with finite cross sections were evaluated. In order to treat axially nonsymmetrical fibers such as HFs with air holes arranged in a triangular lattice in the cladding region, the second moment of the optical intensity distribution was introduced as the definition of the effective modal spot size w_{eff} (a half of MFD). We have shown that A_{eff} and w_{eff} are almost independent of the number of rings of air holes and that the relation $A_{eff} = \pi w_{eff}^2$ does not always hold, especially in smaller air filling fraction and/or longer wavelengths. In addition, we have found that for HFs with large air holes operating at longer wavelengths, the mode profiles of the two linearly polarized fundamental modes are significantly different from each other. The values of A_{eff} and MFD obtained here were effectively applied to evaluating the beam divergence and the nonlinear phase shift of HFs. The applicability of A_{eff} and MFD to the splice loss, bending loss, and source-to-fiber coupling efficiency are now under consideration.